Research in Astronomy and Astrophysics, 24:125008 (10pp), 2024 December https://doi.org/10.1088/1674-4527/ad8a08

A Photometric and Astrometric Study of Open Star Clusters FSR-163 and Majaess 215 Using Gaia DR3

Ola Ali[1], A. L. Tadross[1], A. I. Osman[1], and Z. M. Hayman[2]
[1] Astronomy Department, National Research Institute of Astronomy and Geophysics, 11421, Helwan, Cairo, Egypt; ola.ali@nriag.sci.eg
[2] Astronomy Department, Faculty of Science, Cairo University, 12613, Giza, Egypt
Received 2024 September 7; revised 2024 October 16; accepted 2024 October 18; published 2024 December 2

Abstract

We have examined most of the astrophysical properties of the two star clusters, FSR-163 and Majaess 215, using the third data release of the Gaia space mission (Gaia DR3). We utilized the pyUPMASK method to allocate the probabilities of stars' membership candidates. Using the clusters' trigonometric parallaxes of the members with probabilities $P > 50\%$, we calculated the distance to the clusters of 3290 ($\pm$140) and 2833 ($\pm$140) pc, respectively, which match well with our isochrone fitting results on the color–magnitude diagrams. We determined the age of the clusters, and they are 1.00 ($\pm$0.15) and 3.55 ($\pm$0.15) Gyr for FSR-163 and Majaess 215, respectively. We evaluated the following photometric parameters: reddenings, distances, galactic geometrical distances, luminosity–mass functions, and total masses of the two clusters. On studying the dynamic state of the two clusters, we found that Majaess 215 is more relaxed than FSR-163.

Key words: (Galaxy:) open clusters and associations: individual (FSR-163 and Majaess 215) – proper motions – stars: luminosity function – mass function – catalogs – Astronomical Databases

1. Introduction

Any shapeless concentration of young stars that is bounded by their gravitational forces is commonly known as an open cluster (OC). These are groups of stars consisting of about a few thousand stars whose formation originated from the same molecular cloud, and their gravitational bounding is still active; most observed OCs are in spiral and irregular galaxies, where the active star formation process is in progress. The current study's motivation is an attempt to determine the Milky Way's Galactic disk structure and evolution (Gilmore et al. 2012; Moraux 2016). They additionally enable us to make comparisons between our Galaxy and other surrounding galaxies, including the Magellanic Clouds (Efremov & Elmegreen 1998). The Gaia mission (Gaia Collaboration et al. 2016) is a useful addition to our tools for studying OCs with high accuracy (Gaia Collaboration et al. 2018; Cantat-Gaudin 2022).

Gaia is an abbreviation for Global Astrometric Interferometer for Astrophysics. Gaia Data Release 3 (Gaia DR3) provides accumulated observations of OC parameters such as equatorial coordinates, proper motions, and trigonometric parallaxes for over 1.8 billion sources (Gaia Collaboration et al. 2023). Additionally, G, G_{BP}, and G_{RP} photometric filters and color indices for around 1.5 billion sources are provided (http://www.cosmos.esa.int/gaia).

Though about 7000 objects classified as Galactic OCs (Hunt & Reffert 2023), only about half of them have been studied in detail (Tadross 2018). Gaia DR3 has added new candidate OCs which are waiting to be confirmed through photometric and astrometric studies (Kharchenko et al. 2013).

FSR-163 is a member of the Froebrich OCs list (Kharchenko et al. 2013), and Majaess 215 is also on the Majaess OCs list (Majaess 2013). Both are regarded as poorly studied clusters, where FSR-163 is mentioned in some catalogs with its position only and has some parameters that were studied by Kharchenko et al. (2013), i.e., before the Gaia database was released. Table 1 contains a comparison between the current estimated parameters of FSR-163 and those of Kharchenko et al. (2013). Our goal is to investigate such objects using Gaia DR3, which provides more accurate physical characteristics, e.g., distances and kinematics of the clusters' members.

The structure of the present article can be summarized as follows. In Section 2, the extracted data and their treatments are reported. The exact corrected positions and real sizes are declared in Section 3. Section 4 presents the membership and color–magnitude diagrams (CMDs). The mass and luminosity functions as well as the relaxation time are evaluated in Section 5. In conclusion, Section 6. summarizes our study and inventory of the calculated parameters.

2. Data Treatments

Using the Gaia DR3 database (Gaia Collaboration et al. 2023), astrometric and photometric analyses of both OCs FSR-163 and Majaess 215 are processed. The extracted data are limited by a 20′ radius with a center located at the SIMBAD central coordinates of the objects under consideration http://simbad.u-strasbg.fr/simbad/; which are also listed in Dias et al. (2014), see https://vizier.cds.unistra.fr/viz-bin/VizieR-3?-source=I/355/gaiadr3 for the source data.

Table 1
A Comparison Between Our Estimated Parameters for FSR-163 and Those of Kharchenko et al. (2013)

Parameter	Current Study	Kharchenko et al. (2013)
α_{J2000} (hh:mm:ss)	20:00:19	20:00:21
δ_{J2000} (dd:mm:ss)	+25:25:16	+25:25:12
l_{J2000} (°)	63.22417	63.222
b_{J2000} (°)	−2.41962	−2.423
Log age (yr)	9.0	8.55
d (pc)	3290	3412
$E(B-V)$ (mag)	0.68	1.04
R_{lim}(arcmin)	8.5	6.6
R_c (pc)	0.63	0.95
R_t (pc)	13.78	15.49

As a consequence, we extracted photometric and astrometric data for the two OCs including the stars' equatorial coordinates (α, δ), proper-motion components ($\mu_\alpha \cos\delta$, μ_δ), trigonometric parallaxes (ϖ), apparent G magnitudes, and their color indices with magnitude limit of $G \approx 22$ mag. FSR-163 is a southern OC located within the boundaries of the constellation Vulpecula. At J2000.0, FSR-163 has the following coordinates: $\alpha = 20^h00^m19^s$, $\delta = +25°25'16''$, $l = 63.^\circ2242$, $b = -2.^\circ4196$. Majaess 215 is a northern OC located within the boundaries of the constellation Cepheus. At J2000.0, Majaess 215 has the following coordinates: $\alpha = 22^h49^m34^s$, $\delta = +59°56'9''$, $l = 108.^\circ2157$, $b = +0.^\circ5929$.

Figure 1 is a representation of optical images for both OCs as referenced from the colored Digitized Sky Survey (DSS) image of ALADIN https://aladin.u-strasbg.fr/AladinLite, where the fields of view (FOV) are 9.14 and 5.′72 for both OCs. The number of stars counted with magnitude limits of $7 < G < 22$ mag are 69,031 stars for FSR-163, and 20,501 stars with magnitude limits of $6 < G < 22$ mag for Majaess 215. The photometric completeness limits (PCLs) were estimated for both clusters to increase the accuracy of the astrophysical parameters obtained. The stars with magnitudes less than PCL have been excluded (the Plx and PM errors are increasing exponentially with magnitude). To calculate PCL, G apparent magnitude histograms were established for each OC as shown in Figure 2. The mean error is ∼1 mas in Plx, and ∼1 mas yr^{-1} in PM components. The convenience of a source and single-star model can be indicated using the renormalized unit weight error (RUWE), and all the stars with RUWE > 1.4 are excluded to use the standard sources. Also, the stars with negative parallaxes ($\varpi < 0$ mas) are excluded.

On the other hand, RUWE, or "renormalized unit weight error" is a parameter used in the astrometric data of the Gaia mission, to assess the quality of the measurements. It provides a measure of how well the positional measurements of stars match their predicted positions based on a single-star model. If a binary star system is not resolved into individual stars during astrometric observations, the measurements can be contaminated, resulting in higher RUWE values, and implying poor astrometric quality. Therefore, all the stars with RUWE > 1.4 were excluded (Lindegren et al. 2018).

Figure 3's left-hand side is a vector point diagram (VPD) within the limited radius of each OC as estimated in Section 3 using the Virtual Observatory tool, TOPCAT (Taylor 2005). A homogeneous area around the darkest part of the VPD is selected for each OC (Bragaglia 2018). Our given data were reduced to two groups of 5696 and 1433 stars for FSR-163 and Majaess 215, respectively. The mean proper-motion components ($\mu_\alpha \cos\delta$, μ_δ) are found to be $(-2.76 \pm 0.46, -5.11 \pm 0.61)$, and $(-2.89 \pm 0.74, -2.00 \pm 0.42)$ mas yr^{-1} for FSR-163 and Majaess 215, respectively.

To assign the probable members of the studied clusters, we used the Unsupervised Photometric Membership Assignment in Stellar Clusters (pyUPMASK)[3] algorithm which is a Python open-source software package (Cantat-Gaudin & Anders 2020; Pera et al. 2021) pyUPMASK is a Python open-source software package algorithm used to determine the membership probability of stars in a cluster. It employs a combination of k-means clustering and statistical analysis to identify cluster members based on their five-dimensional parametric space that includes equatorial coordinates (α, δ), proper-motion components ($\mu_\alpha \cos\delta$, μ_δ), and trigonometric parallaxes (ϖ). The k-means algorithm partitions the data into k-initial clusters, where each star is assigned to the cluster with the nearest mean value. After the initial clustering, pyUPMASK iteratively refines the membership probabilities. In each iteration, the algorithm evaluates the likelihood that each star belongs to its assigned cluster. The iterative process continues until the membership probabilities converge. Stars with higher membership probabilities are more likely to be true cluster members, see Yontan et al. (2023) and Gokmen et al. (2023). We selected $P \geqslant 50\%$ which we regarded to be the lower limit for the membership probability. After a large number of iterations, we identified 1385 and 395 stars as the most likely members for FSR-163 and Majaess 215 respectively. Hence, we checked the resultant members on the comoving diagram of each OC, as illustrated on the right-hand side of Figure 3, which affirms the constancy of speed and direction of all membership candidates. Figure 4's right-hand panels illustrate a histogram of the trigonometric parallaxes of both OCs as well as the magnitude-parallax relation for membership candidates.

Lindegren et al. (2021) reported a code for the zero-point offset of the Gaia Early Data Release 3 (EDR3) parallaxes.[4] The zero-point correction was approximated as a function of G-magnitude, ecliptic latitude, and color (using ν_{eff} for the five-parameter solutions and pseudo-color for the six-parameter

[3] https://github.com/msolpera/pyUPMASK
[4] https://gitlab.com/icc-ub/public/gaiadr3_zeropoint

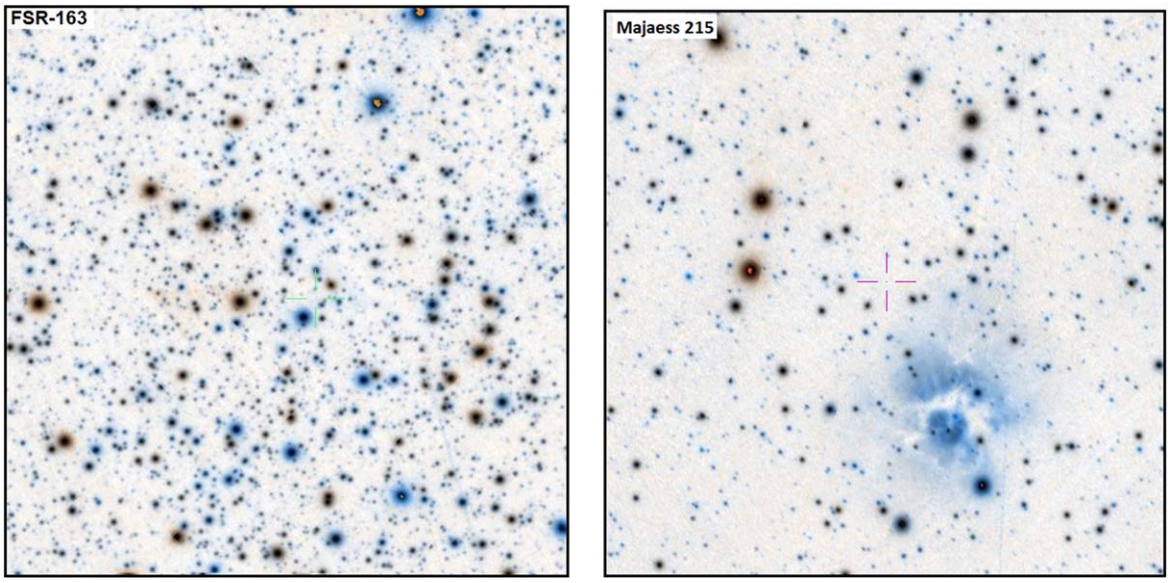

Figure 1. The optical images of FSR-163 and Majaess-255 as taken from ALADIN at DSS colored optical wavelength and FOV of $9\farcm14$ and $5\farcm72$ respectively, North is up, East is to the left.

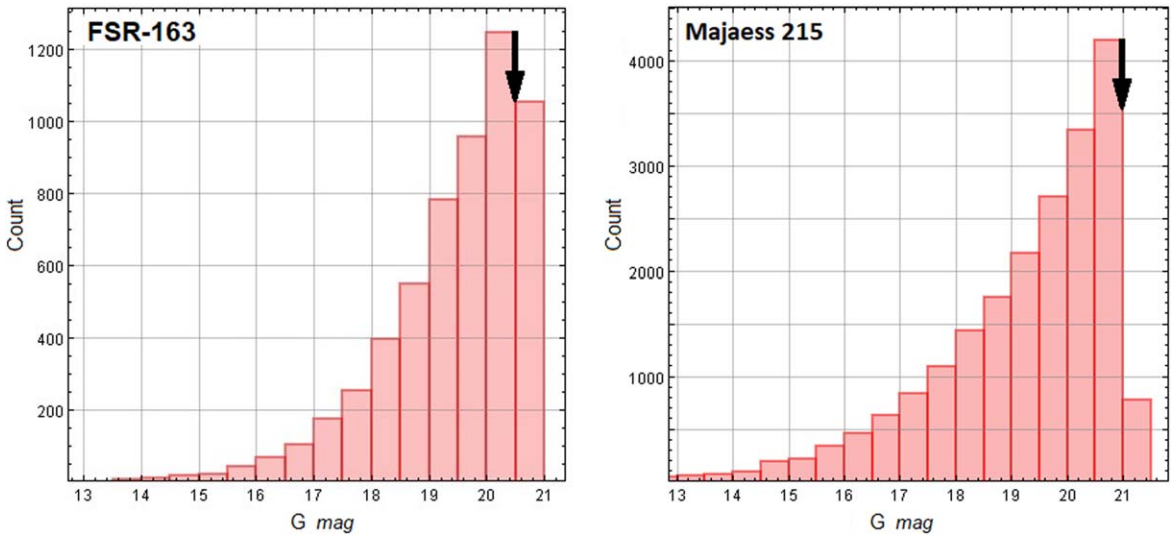

Figure 2. Interval *G* band magnitude histograms of FSR-163 and Majaess 215. The arrows show the adopted completeness limiting magnitudes of 20.5 and 21.0 mag for FSR-163 and Majaess 215, respectively.

solutions). Applying this code to the likely members of each studied cluster, the corrected parallaxes are found to be 0.304 ± 0.010 and 0.353 ± 0.013 mas for FSR-163 and Majaess 215, respectively. These lead to derived distances of $\sim$3290 ($\pm$80) and $\sim$2833 ($\pm$80) pc, respectively.

3. True Centers and Sizes

The densest location within the OC defines where the cluster center is located. The data we used to conduct our analysis were obtained from the Gaia DR3 database. We divided the OC into equal-sized bins and calculated the number of stars in each bin. As demonstrated in Figure 5, three-dimensional kernel density analysis was applied to derive the center values of FSR-163 and Majaess 215. The calculated coordinates and SIMBAD values coincide well. For FSR-163 and Majaess 215, the discrepancies in R.A. and decl. are found to be 3 s and $12'$ and 20 s and $9''$ respectively. Hence, it is possible to disregard the small uncertainty in position (l, b) of both OCs.

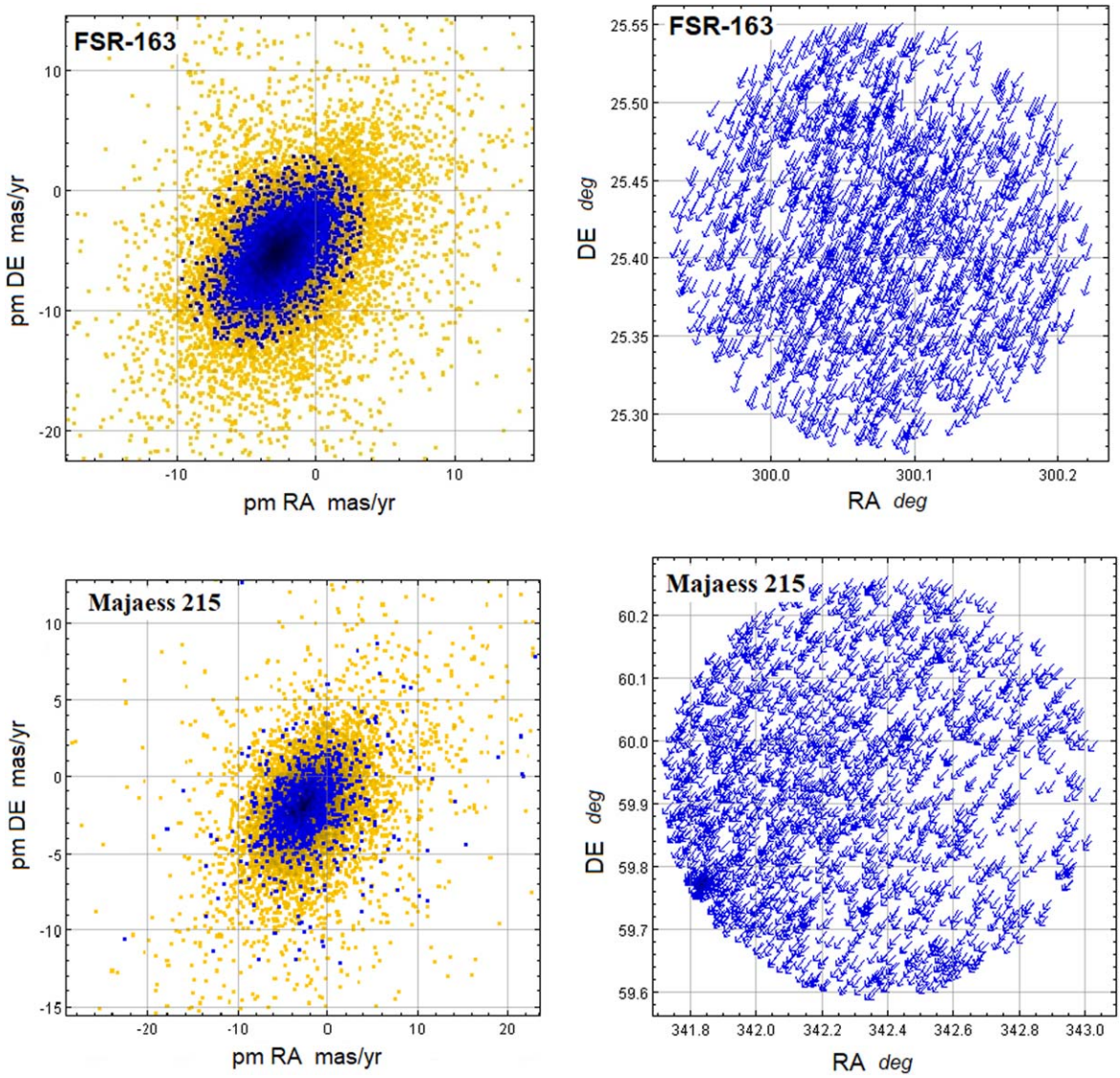

Figure 3. The left-hand panels show the VPDs of the stars in FSR-163 and Majaess 215. The blue points refer to the cluster stars inside their limited radius, while the yellow points refer to the background field. The right-hand panels show the likely members as comoving stars in each cluster, i.e., those stars that move together at the same speed and direction in the sky.

The OC's radial density profile (RDP) can be found by counting the stars in each radial bin. We can easily calculate the density of each zone by dividing the number of stars in each zone by its surface area (Tadross 2018, 2023; Tadross & Elhosseiny 2022). The OC's surface density profile often exhibits a gradual decline from its core toward the outer regions. The limiting radius $R_{\rm lim}$ of a certain cluster is usually defined as the radius at which the RDP becomes constant. We can calculate the error of each bin using Poisson noise $\frac{1}{\sqrt{N}}$, where N is the number of stars in each bin, as demonstrated in Figure 6. We applied the King model to each cluster (King 1966), which has the following formula

$$f(R) = f_{bg} + \frac{f_0}{1 + \left(\frac{R}{R_c}\right)^2},$$

where f_{bg} is the background density, f_0 is the central density, and R_c is the cluster's core radius. The RDP begins to decline from the center outward and at a certain point it flattens out. This flattening happens when cluster density diminishes, and the background field density dominates.

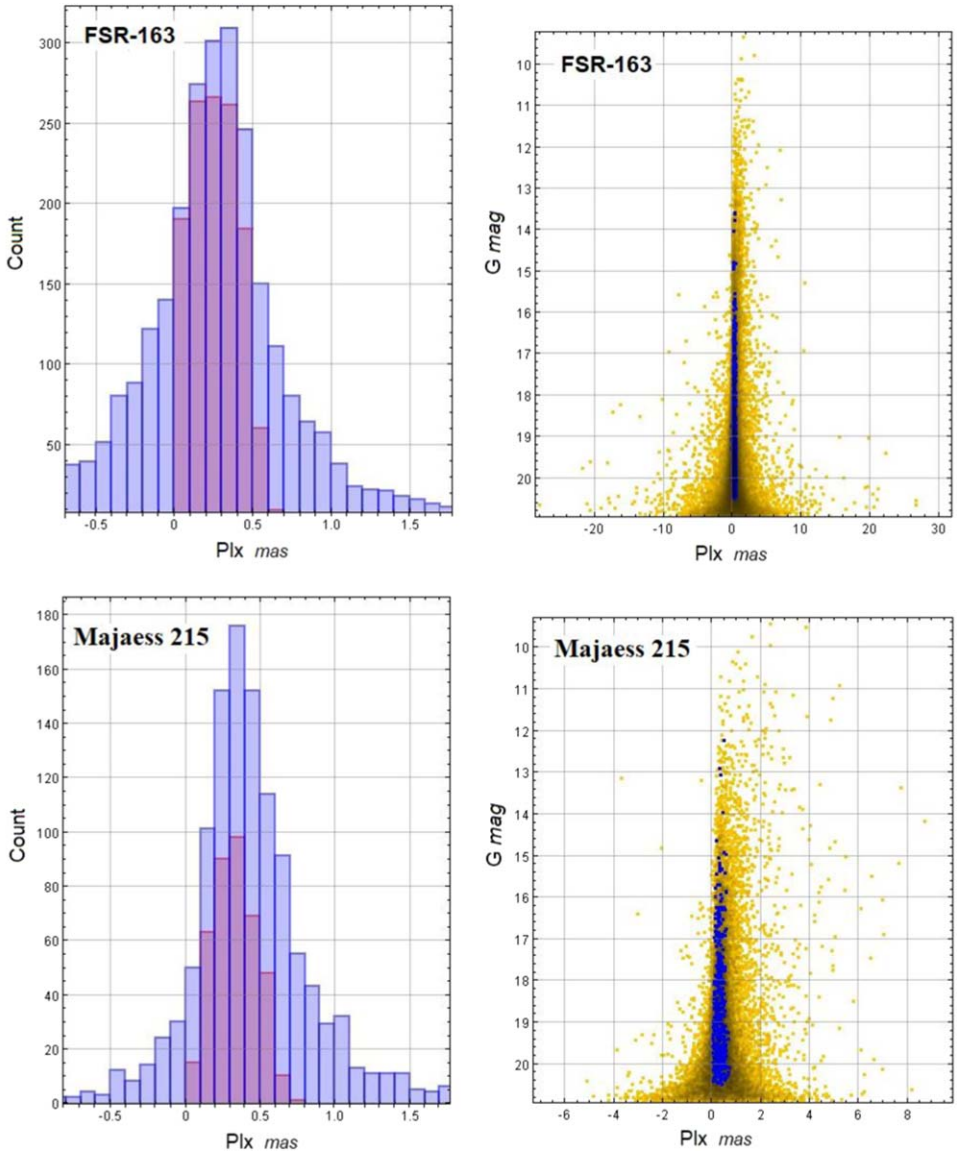

Figure 4. The left-hand panels show the parallaxes of FSR-163 and Majaess 215. The purple histograms refer to the cluster's likely members in the limited cluster region after applying the parallax correction. The blue histograms refer to the background field stars within the same regions. The right-hand panels represent the relationship between the magnitude and parallax of each cluster, where the cluster's likely members (the blue points) with $P > 50\%$ are more concentrated than the background field stars (the yellow points) are.

As shown in Figure 6, for both OCs under consideration, the blue arrows represent the following:

1. The background field star density f_{bg}.
2. Core radii R_c.
3. The limited radii $R_{\rm lim}$.
4. The tidal radii R_t.

The resultant limited radius $R_{\rm lim}$ of FSR-163 is 8.5 ($\pm$0.25) arcmin and that for Majaess 215 is 5.5 ($\pm$0.25) arcmin. The core radius R_c is defined as the distance at which the stellar density value is equal to half of the central density. The resultant R_c for FSR-163 is 0.66 ($\pm$0.11) arcmin and that for Majaess 215 is 0.60 ($\pm$0.11) arcmin. On the other hand, the tidal radius R_t is defined as the distance from the OC at which the gravitational influence of the Galaxy is equivalent to that of the OC core. Using Jeffries' equation (Jeffries et al. 2001),

$$R_t = 1.46 \times (M_c)^{1/3},$$

where R_t is the tidal radius (pc) and M_c is the OC's total mass ($M_\odot$) (as determined in Section 5). The resultant R_t for FSR-163 is 15.2 ($\pm$10) pc and 9.95 ($\pm$10) pc for Majaess 215.

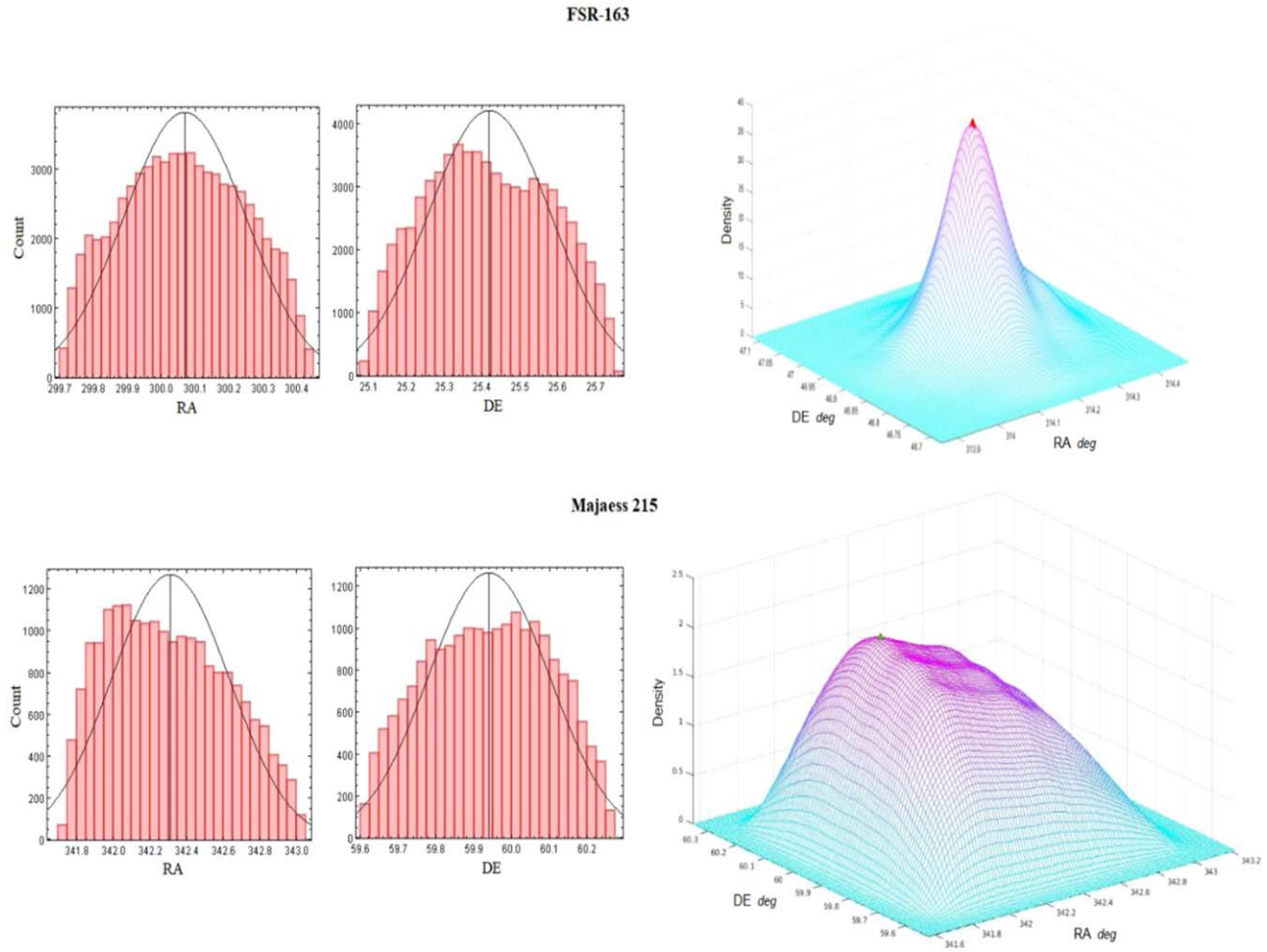

Figure 5. The coordinates of the centers, obtained by applying a Gaussian profile with a three-dimensional kernel density for FSR-163 and Majaess 215, are found to be in good agreement with SIMBAD's centers. The differences of R.A. and decl. are found to be 3 s and 12″ and 20 s and 9″ for FSR-163 and Majaess 215 respectively.

The concentration parameter, $C = \log(R_{\rm lim}/R_c)$, of Peterson and King (Richstone & Tremaine 1986) shows how the OC is distinguished in comparison to the background field stars. It is found to be 1.11 and 0.96 for FSR-163 and Majaess 215, respectively, i.e., FSR-163 has more condensation at its center than Majaess 215.

4. Color–Magnitude Diagrams

The CMD is the instrumental gateway to determining the fundamental characteristics of members of OCs. Based on the Padova stellar isochrones database http://stev.oapd.inaf.it/cgi-bin/cmd, the PARSEC stellar evolutionary isochrones (Bressan et al. 2012) and tracks (Chen et al. 2014; Tang et al. 2014) are utilized with the Gaia filter passbands of Evans et al. (2018) for solar metallicity $Z = 0.0152$. An OC's CMD, age, distance modulus, and reddening can be estimated by obtaining a diagram's fitting. Considering the visual fit displayed in Figure 7, the crucial photometric properties of FSR-163 and Majaess 215 are confirmed with ages of 1.00 (±0.15) and 3.55 (±0.15) Gyr, respectively. The distance moduli were estimated as 12.59 (±0.20) and 12.26 (±0.20) mag, while the reddening ($E(G_{\rm BP} - G_{\rm RP})$) was estimated as 0.95 (±0.10) and 0.80 (±0.10) mag for FSR-163 and Majaess 215, respectively. These values aligned with the mean estimated parallaxes. The computed values of $E(B - V)$ are determined to be 0.68 (±0.10) and 0.57 (±0.10) mag for FSR-163 and Majaess 215, respectively. Based on the CMD-3.6 input form http://stev.oapd.inaf.it/cgi-bin/cmd, the passbands of the Gaia filters G, $G_{\rm BP}$, and $G_{\rm RP}$ are obtained as the following values (Cardelli et al. 1989):

Filter	G	$G_{\rm BP}$	$G_{\rm RP}$
A_λ/A_v	0.83627	1.08337	0.63439

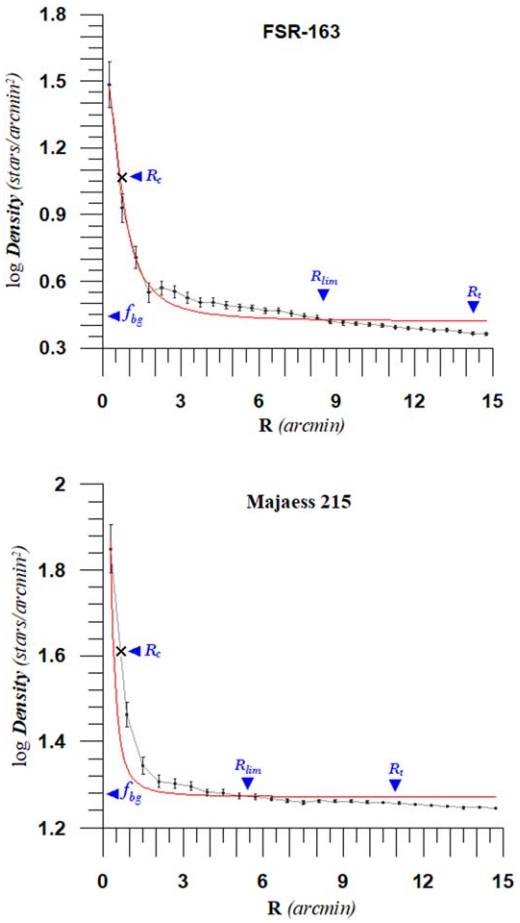

Figure 6. RDPs of FSR-163 and Majaess 215. The error bars refer to the Poisson distribution $1/N$, and the red line refers to the fitted profile of King (1966). The blue arrows refer to the background field (f_{bg}), core radius (R_c), limited radius ($R_{\rm lim}$), and tidal radius (R_t) of each cluster, as labeled respectively. The limited radius is found to be 8.5 (±0.25) and 5.5 (±0.25) arcmin for FSR-163 and Majaess 215, respectively.

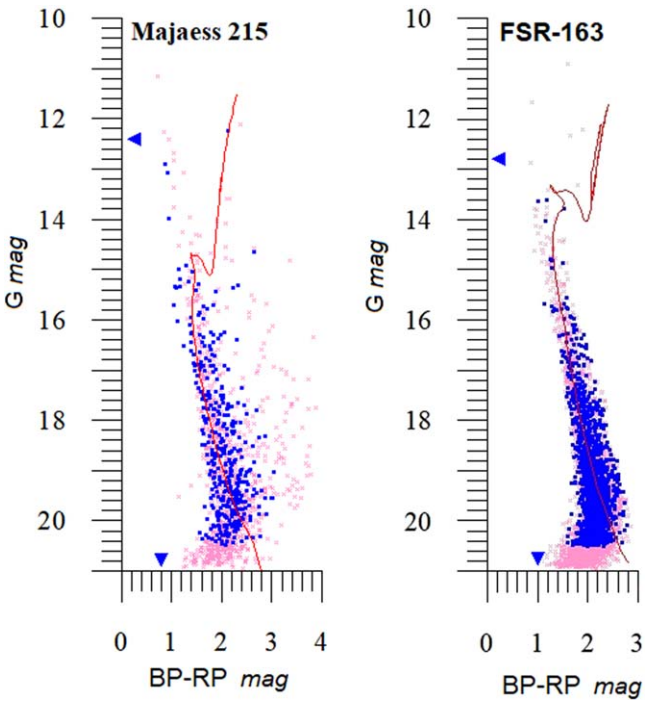

Figure 7. CMDs of FSR-163 and Majaess 215 fitted with theoretical PARSEC isochrones of ages 1.00 (±0.15) and 3.55 (±0.15) Gyr, respectively. The blue points refer to the likely member stars ($P > 50\%$), while the pink points refer to the background field stars inside the limited radius. The small triangles indicate the values of the distance modulus and reddening. The distance modulus ($m - M$) is found to be 12.59 (±0.20) and 12.26 (±0.20) mag respectively. The reddening $E(G_{\rm BP} - G_{\rm RP})$ is found to be 0.95 (±0.10) and 0.80 (±0.10) mag for both clusters, respectively.

We get $AG_{\rm BP} = 1.083\,A_\nu$, $AG_{\rm RP} = 0.634\,A_\nu$, and $A_G = 0.836\,A_\nu$, then $A_\nu = 2.227\ E(G_{\rm BP} - G_{\rm RP})$ and $A_G = 1.862\ E(G_{\rm BP} - G_{\rm RP})$. By converting the color excess to $E(B - V)$ and correcting the magnitudes for interstellar reddening, these ratios have been employed with $A_\nu = R_\nu E(B - V)$, where $A_\nu = 3.1$, (Zhong et al. 2019).

The computed values of $E(B - V)$ are determined to be 0.68 (±0.10) and 0.57 (±0.10) mag for FSR-163 and Majaess 215, respectively.

The distance between the Galactic center and the Sun (R_0) is given to be 8.2 kpc (Bland-Hawthorn & Gerhard 2016). Based on Tadross (2011), the Cartesian galactocentric positions ($X_\odot - Y_\odot - Z_\odot$) are calculated for FSR-163 and Majaess 215. According to Lynga (1982), the Y-axis connects the Sun to the Galactic center (positive toward the Galactic anti-center), while the X-axis is perpendicular to the Y-axis (positive in the first and second Galactic quadrants), and Z-axis is the distance from the Galactic plane, see Table 2. The distance from the Galactic center (R_g) can be calculated using R_0 and ($X_\odot - Y_\odot - Z_\odot$) as follows

$$R_g = \sqrt{(R_0 - X_\odot)^2 + {Y_\odot}^2 + {Z_\odot}^2}.$$

5. Luminosity, Mass Functions, and Dynamical States

The luminosity and mass functions (LF and MF) can be conducted using data on candidates' membership in FSR-163 and Majaess 215. LF is the count of stars in an absolute magnitude interval, while MF is the count of stars in a logarithmic mass interval. The study of LF and MF faces difficulties which are to exclude the field star contamination from the OC region. Therefore, the LF and MF of each OC are affected by the number of its membership candidates.

Overcoming the difficulties, we should:

1. Determine the luminosity and mass of each membership candidate. Thus, the distance modulus of each OC is employed to convert apparent magnitudes into absolute magnitudes.

Table 2
The Current Estimations of the Clusters' Properties

Parameter	FSR-163	Majaess 215
α_{J2000} (hh:mm:ss)	20:00:19	22:49:34
δ_{J2000} (dd:mm:ss)	+25:25:16	+59:56:09
l_{J2000} (°)	63.22417	108.2157
b_{J2000} (°)	−2.41962	+0.5929
Age (Gyr)	1.00 ± 0.15	3.55 ± 0.15
$(m - M)_o$ (mag)	12.59 ± 0.20	12.26 ± 0.20
Dist. (pc)	3290 ± 140	2833 ± 140
Z	0.0152	0.0152
Plx. (mas)	0.304 ± 0.010	0.353 ± 0.013
$E(G_{BP} - G_{RP})$ (mag)	0.95 ± 0.10	0.80 ± 0.10
A_G (mag)	1.77 ± 0.12	1.50 ± 0.12
$E(B - V)$ (mag)	0.68 ± 0.10	0.57 ± 0.10
Mem. Stars	1365 ± 50	370 ± 20
R_{lim} (arcmin)	8.5 ± 0.25	5.5 ± 0.25
R_c (arcmin)	0.66 (∼0.63 pc)	0.60 (∼0.49 pc)
R_t (arcmin)	14.4 (∼13.78 pc)	11.0 (∼9.06 pc)
C	1.11	0.96
pmRA (mas/yr)	-2.76 ± 0.46	-2.89 ± 0.74
pmDE (mas/yr)	-5.11 ± 0.61	-2.00 ± 0.42
R_g (Kpc)	7.37	9.46
$X_\odot$ (pc)	−1481	886
$Y_\odot$ (pc)	2935	2691
$Z_\odot$ (pc)	−139	29
IMF slope	−2.40	−3.70
T. Lum. (mag)	-2.40 ± 0.25	-1.94 ± 0.25
T. mass ($M_\odot$)	1125 ± 90	320 ± 60
T_R (Myr)	111	58
τ	9	61

2. Developing two polynomial equations based on the main sequence data of the employed isochrones [M_G versus log L and M_G versus mass $\mathcal{M}$].

The evolution tracks theoretical tables of Marigo et al. (2017) at the OC's age have been used and the total mass and total luminosity are determined (summing the number of membership candidates' multiplied in each bin by the appropriate values (L and $\mathcal{M}$) of that bin) (Tadross 2012).

Histograms of LF for FSR-163 and Majaess 215 are illustrated in the left-hand panels of Figure 8, while the MF relations are illustrated in the right-hand panels. It is noticeable that the fainter and less massive stars are dispersed outside of the OCs, while the brightest and most massive stars are concentrated at the center. The total luminosity in the G-filter is found to be −2.40 (±0.25) and −1.94 (±0.25) mag for FS-163 and Majaess 215, respectively. The slope of the well-known equation for the initial mass function (IMF) is represented by the linear fit

$$\log \frac{dN}{dM} = -\alpha \log(M) + \text{const.}$$

Here $\frac{dN}{dM}$ is the star count in the mass interval [M: $M + dM$] and α is the linear slope of the relation, which indicates that the estimated masses of a standard OC lie in the range of mean value ($\alpha \approx -2.35$) (Salpeter 1955). From the right-hand panels of Figure 8, we notice that the observed IMF for FSR-163 and Majaess 215 agree with Salpeter (1955)'s value (−2.40 and −3.70, respectively), within the error bars of Poisson noise $\frac{1}{\sqrt{N}}$ where N is the star count in each bin. However, the overall masses are found to be $1125 \pm 90\,M_\odot$ and $320 \pm 60\,M_\odot$ for FSR-163 and Majaess 215, respectively.

However, the relaxation time (T_R) is the duration required by the OC to self-assemble and stabilize in the face of annihilation forces. T_R is the timescale, mostly determined by the OC's mass and membership candidates' count, at which all traces of its initial conditions are lost. Using the formula of Spitzer & Hart (1971), the relaxation time may be computed as follows

$$T_R = \frac{8.9 \times 10^5 \times \sqrt{N} \times R_h}{\sqrt{\langle \bar{m} \rangle} \times \log(0.4 \times N)},$$

where N is the membership candidates' count of the OC, R_h is the radius containing half of the OC's mass (pc), and $\langle \bar{m} \rangle$ is the average mass of each membership candidate ($M_\odot$). Assuming R_h equals half of the OC limiting radius, T_R is found to be 111 and 58 Myr for FSR-163 and Majaess 215, respectively. The

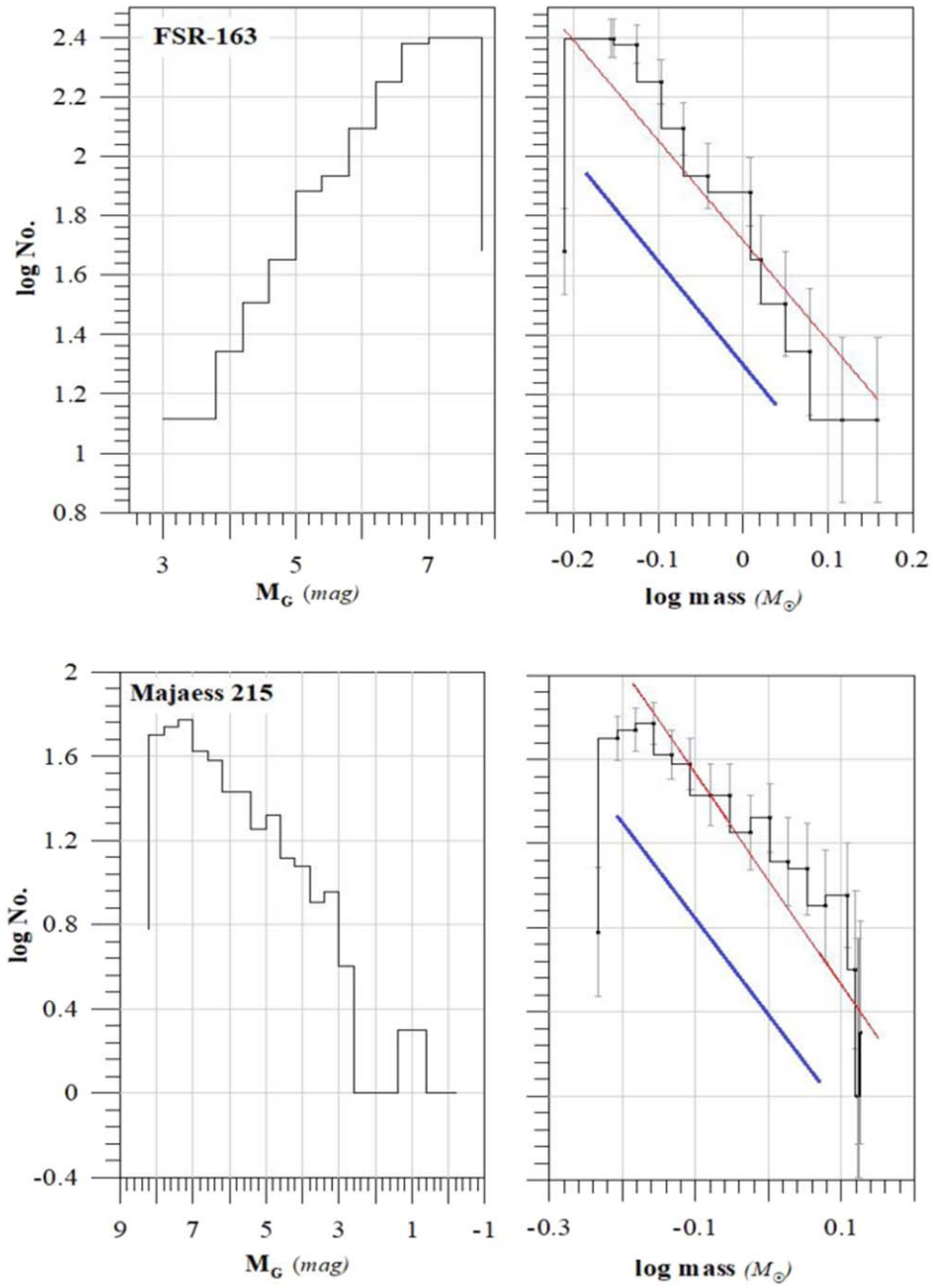

Figure 8. The left-hand panels represent the luminosity function distributions of FSR-163 and Majaess 215. The right-hand panels represent the mass function distributions with error bars for both clusters. The error bars refer to the Poisson distribution $1/\sqrt{N}$. The blue thick line refers to the calculated IMF slope of Salpeter (1955), where $\alpha \approx -2.35$. It matches well with the linear fit (red line) of FSR-163, where its IMF slope is about -2.40; while it matches somewhat with Majaess 215, where its IMF slope is about -3.70.

dynamical evolution parameter τ can be defined as $\tau = \mathrm{Age}/T_R$. If the OC's age is older than the relaxation time, i.e., $\tau \gg 1.0$, then the OC is dynamically relaxed, and vice versa. In our case, we found that $\tau \approx 9$ and 61 for FSR-163 and Majaess 215, respectively. It is clear that Majaess 215 is more relaxed than FSR-163.

6. Conclusions

We presented here a comprehensive Gaia DR3 study of the two poorly studied OCs FSR-163 and Majaess 215. These OCs lie in the southern and northern sky, in constellations Vulpecula and Cepheus, respectively. The membership probabilities of

stars were assigned by using the pyUPMASK algorithm. Most of the astrophysical parameters of both clusters have been estimated. For the sake of accuracy, we applied the ASteCA code (Perren et al. 2015, 2020) https://asteca.readthedocs.io/en/latest/ to both clusters and found that our values of the estimated parameters agree with ASteCA. However, all the OCs' essential physical characteristics are listed in Table 2.

Acknowledgments

The work made use of data from the European Space Agency (ESA) mission Gaia https://www.cosmos.esa.int/Gaia, processed by the Gaia Data Processing and Analysis Consortium (DPAC, https://www.cosmos.esa.int/web/Gaia/dpac/consortium). Funding for the DPAC was provided by national institutions, particularly those participating in the Gaia Multilateral Agreement. This work made use of the SIMBAD database and the VizieR catalog access tool, operating at the CDS, Strasbourg, France (DOI:10.26093/cds/vizier), and of NASA Astrophysics Data System Bibliographic Services.

ORCID iDs

Ola Ali https://orcid.org/0000-0002-0213-3232
A. L. Tadross https://orcid.org/0000-0001-7090-3684

References

Bland-Hawthorn, J., & Gerhard, O. 2016, ARA&A, 54, 529
Bragaglia, A. 2018, in IAU Symp., 330, Astrometry and Astrophysics in the Gaia Sky, ed. A. Recio-Blanco et al. (Cambridge: Cambridge Univ. Press), 119
Bressan, A., Marigo, P., Girardi, L., et al. 2012, MNRAS, 427, 127
Cantat-Gaudin, T. 2022, Universe, 8, 111
Cantat-Gaudin, T., & Anders, F. 2020, A&A, 633, A99
Cardelli, J. A., Clayton, G. C., & Mathis, J. S. 1989, ApJ, 345, 245
Chen, Y., Girardi, L., Bressan, A., et al. 2014, MNRAS, 444, 2525
Dias, W. S., Monteiro, H., Caetano, T. C., et al. 2014, A&A, 564, A79
Efremov, Y. N., & Elmegreen, B. G. 1998, MNRAS, 299, 588
Evans, D. W., Riello, M., De Angeli, F., et al. 2018, A&A, 616, A4
Gaia Collaboration, Babusiaux, C., van Leeuwen, F., et al. 2018, A&A, 616, A10
Gaia Collaboration, Brown, A. G. A., Prusti, T., et al. 2023, A&A, 674, A1
Gaia Collaboration, Prusti, T., de Bruijne, J. H. J., et al. 2016, A&A, 595, A1
Gilmore, G., Randich, S., Asplund, M., et al. 2012, Msngr, 147, 25
Gokmen, S., Eker, Z., Yontan, T., et al. 2023, AJ, 166, 263
Hunt, E. L., & Reffert, S. 2023, A&A, 673, A114
Jeffries, R. D., Thurston, M. R., & Hambly, N. C. 2001, A&A, 375, 863
Kharchenko, N. V., Piskunov, A. E., Schilbach, E., Röser, S., & Scholz, R. D. 2013, A&A, 558, A53
King, I. R. 1966, AJ, 71, 64
Lindegren, L., Bastian, U., Biermann, M., et al. 2021, A&A, 649, A4
Lindegren, L., Hernández, J., Bombrun, A., et al. 2018, A&A, 616, A2
Lynga, G. 1982, A&A, 109, 213
Majaess, D. 2013, Ap&SS, 344, 175
Marigo, P., Girardi, L., Bressan, A., et al. 2017, ApJ, 835, 77
Moraux, E. 2016, Stellar Clusters: Benchmarks of Stellar Physics and Galactic Evolution - EES2015, 80-81 ed. E. Moraux, Y. Lebreton, & C. Charbonnel (London: EAS Publication Series), 73
Pera, M. S., Perren, G. I., Moitinho, A., Navone, H. D., & Vazquez, R. A. 2021, A&A, 650, A109
Perren, G. I., Giorgi, E. E., Moitinho, A., et al. 2020, A&A, 637, A95
Perren, G. I., Vázquez, R. A., & Piatti, A. E. 2015, A&A, 576, A6
Richstone, D. O., & Tremaine, S. 1986, AJ, 92, 72
Salpeter, E. E. 1955, ApJ, 121, 161
Spitzer, L. J., & Hart, M. H. 1971, ApJ, 164, 399
Tadross, A. L. 2011, JKAS, 44, 1
Tadross, A. L. 2012, NewA, 17, 198
Tadross, A. L. 2018, RAA, 18, 158
Tadross, A. L. 2023, AN, 344, e20230073
Tadross, A. L., & Elhosseiny, E. G. 2022, RMxAA, 58, 387
Tang, J., Bressan, A., Rosenfield, P., et al. 2014, MNRAS, 445, 4287
Taylor, M. B. 2005, in ASP Conf. Ser. 347, Astronomical Data Analysis Software and Systems XIV, ed. P. Shopbell, M. Britton, & R. Ebert (San Francisco, CA: ASP), 29
Yontan, T., Bilir, S., Çakmak, H., et al. 2023, AdSpR, 72, 1454
Zhong, J., Chen, L., Kouwenhoven, M. B. N., et al. 2019, A&A, 624, A34